Sedimentary ancient DNA from Kronotsky Peninsula: how sea ice, salinity and insolation dynamics have shaped diatom composition and richness over the past 20,000 years

H. H. Zimmermann[1], K. R. Stoof-Leichsenring[1], S. Kruse[1], D. Nürnberg[2], R. Tiedemann[3], and U. Herzschuh[1,4,5]

[1]Polar Terrestrial Environmental Systems, Alfred Wegener Institute Helmholtz Centre for Polar and Marine Research, Potsdam, 14473, Germany

[2]Ocean circulation and climate dynamics, GEOMAR Helmholtz Centre for Ocean Research Kiel, Kiel, 24148, Germany

[3]Marine Geology, Alfred Wegener Institute Helmholtz Centre for Polar and Marine Research, Bremerhaven, 27568, Germany

[4]Institute of Biochemistry and Biology, University of Potsdam, 14476 Potsdam, Germany

[5]Institute of Environmental Sciences and Geography, University of Potsdam, 14476 Potsdam, Germany

Corresponding author: Heike H. Zimmermann (heike.zimmermann@awi.de), Ulrike Herzschuh (ulrike.herzschuh@awi.de)

Key Points:

- diatom *sed*aDNA composition is concordant with reconstructed sea-ice dynamics, SSTs and subsurface salinities over the past millenia

- loss of diatom richness at ~11.1 cal kyr BP is possibly a consequence of increased freshwater input from Kamchatka

- shifts of potential ecotypes of species from the genus *Chaetoceros* with changing environmental conditions

Abstract

27

28 We traced diatom composition and diversity through time using diatom derived sedimentary
29 ancient DNA (*sed*aDNA) from eastern continental slope sediments off Kamchatka (North
30 Pacific) by applying a short, diatom-specific marker on 63 samples in a DNA metabarcoding
31 approach. The sequences were assigned to diatoms that are common in the area and
32 characteristic of cold water. *Sed*aDNA allowed us to observe shifts of potential lineages from
33 species of the genus *Chaetoceros* that can be related to different climatic phases, suggesting that
34 pre-adapted ecotypes might have played a role in the long-term success of species in areas of
35 changing environmental conditions. These *sed*aDNA results complement our understanding of
36 the long-term history of diatom assemblages and their general relationship to environmental
37 conditions of the past. Sea-ice diatoms (*Pauliella taeniata* (Grunow) Round & Basson, *Attheya
38 septentrionalis* (Østrup) R.M.Crawford and *Nitzschia frigida* (Grunow)) detected during the late
39 glacial and Younger Dryas are in agreement with previous sea-ice reconstructions. A positive
40 correlation between pennate diatom richness and the sea-ice proxy IP_{25} suggests that sea ice
41 fosters pennate diatom richness, whereas a negative correlation with June insolation and
42 temperature points to unfavorable conditions during the Holocene. A sharp increase in
43 proportions of freshwater diatoms at ~11.1 cal kyr BP implies the influence of terrestrial runoff
44 and coincides with the loss of 42% of diatom sequence variants. We assume that reduced salinity
45 at this time stabilized vertical stratification which limited the replenishment of nutrients in the
46 euphotic zone.

47

48 **1 Introduction**

49   Climate warming is transforming arctic and subarctic ecosystems by a reduction in the

50 duration, extent and thickness of sea ice (Parkinson et al., 1999; Walsh et al., 2017) – a key variable

51 of the global climate system whose disappearance is resulting in a positive temperature feedback

52 from a reduction of the surface albedo (Pistone et al., 2014). Rapidly melting glaciers and increased

53 riverine runoff resulting from thawing permafrost and augmented precipitation over the adjacent

54 continents are expected to decrease sea-surface salinities, for example by about 1.5 ± 1.1 psu on

55 average in the Arctic Ocean (Shu et al., 2018). As a consequence, the fresher, less dense water

56 masses are expected to enhance vertical water-column stratification, which could result in a

57 reduced supply of nutrients to the euphotic zone (Tremblay & Gagnon, 2009). On top of regionally

58 expected loss of sea ice-associated organisms, such a scenario could potentially affect the

59 distribution, composition and diversity of primary producers which are limited by the availability

60 of nutrients, amongst others, with unknown consequences for food-web structure, biochemical

61 cycles and the biological carbon pump (Coupel et al., 2015; Li et al., 2009).

62   The subarctic northwest (NW) Pacific and its adjacent seas have experienced pronounced
63 environmental changes since the Last Glacial Maximum (LGM). The variability of previously
64 reconstructed sea-surface temperatures and sea-ice coverage have been connected to the millennial
65 scale climatic changes recorded in sediment cores from the North Atlantic and in Greenland ice
66 cores (Max et al., 2012; Méheust et al., 2016). Several meltwater pulses have been detected in
67 sediment cores of this region (Gorbarenko et al., 2019), which make it attractive for analyzing the
68 effects of past environmental changes on primary producers.

69   A dominant group of primary producers in high-latitudinal sea-ice and coastal ecosystems
70 are diatoms (Poulin et al., 2011), which are single-celled eukaryotes that form a cell wall of
71 biomineralized silicium dioxide (biogenic silica) and fix carbon dioxide as a product of their
72 photosynthetic activity (Rotatore et al., 1995). They are sensitive to environmental change and can
73 be used as indicators of past sea-surface conditions. For example, morphological data from diatom
74 assemblages of the subarctic NW Pacific and the Bering and Okhotsk Seas have revealed
75 variations in ocean circulation patterns, past distribution of sea ice and past sea-surface
76 temperatures (Caissie et al., 2010; Ren et al., 2009; Sancetta, 1979; Sancetta & Silvestri, 1986;
77 Smirnova et al., 2015). While the investigation of microfossils can distinguish size distributions,
78 resting stages and, in many instances, taxonomic resolution to species level for millions of years
79 back in time, some questions cannot be addressed with morphological data. Amongst others, this
80 includes intra-specific diversity which may be linked to different environmental conditions.

81   The past decade has brought forward genetic surveys which have revealed substantially
82 concealed diversity in diatoms, showing that widely distributed species can have ecotypes
83 associated with, for example, different growth optima (Hamsher et al., 2013) that may not be
84 detected morphologically (cryptic diversity) or only by exhaustive analysis (pseudo-cryptic)
85 (Degerlund et al., 2012). In this regard, the analysis of *sed*aDNA is an advantage. Recently,
86 *sed*aDNA was used as a proxy for sea-ice reconstructions by targeting diatom *sed*aDNA
87 composition (Zimmermann et al., 2019), for tracing a sea-ice dinoflagellate east of Greenland (De
88 Schepper et al., 2019) and to identify changes of ocean circulation patterns by targeting diatoms
89 and non-fossilized foraminifers east of Svalbard (Pawłowska et al., 2020). Ancient DNA has
90 profound advantages. First, it can detect species that are absent from microfossil records either due
91 to dissolution or because they lack a biomineralized cell wall. Second, it allows for the detection
92 of (pseudo-)cryptic diversity in morphological species complexes, which might be adapted to
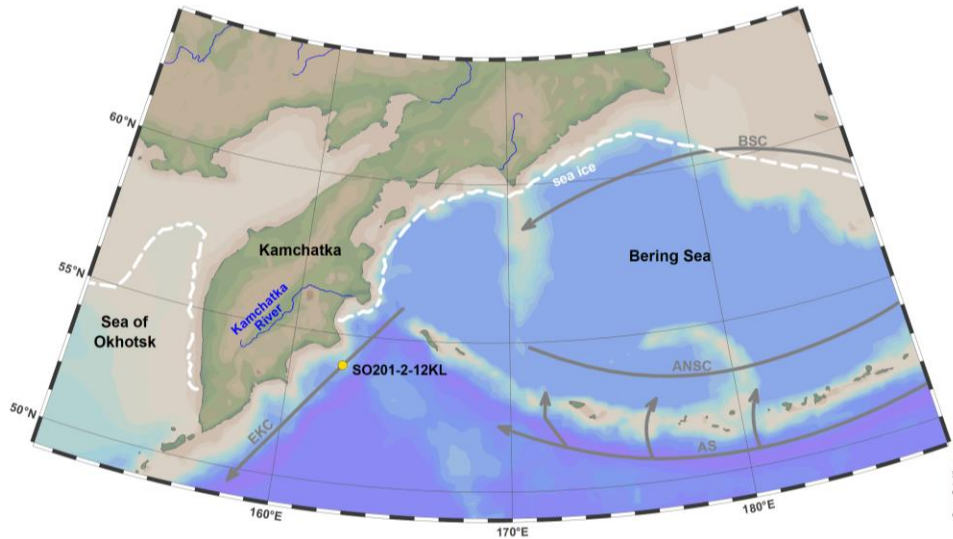
93   different ecological conditions. Third, it is amongst the most applied barcoding gene and thus has

94   a substantial reference database (Rimet et al., 2019; Zimmermann et al., 2014). However, ancient

95   DNA is usually highly degraded (Corinaldesi et al., 2008; Pääbo, 1989). Hence, for DNA

96   metabarcoding of diatoms, the marker should ideally target a short sequence stretch, and

97   additionally avoid co-amplification of other taxonomic groups or co-amplification of highly

98   similar paralogs. Targeting a part of the gene encoding for the large subunit of the RuBisCO (*rbcL*)

99   on the chloroplast genome of diatoms is of advantage. The variability of the *rbcL* gene allows

100 detection of diatoms to species level (Rimet et al., 2019).

101   Our aim is to to trace temporal changes of diatom *sed*aDNA composition and diversity

102 over the past 19.9 cal kyr BP, and to relate changes to environmental conditions to answer the

103 following questions: (1) How has diatom composition changed since the LGM? And how are such

104 changes related to past sea-ice conditions, subsurface salinities and incoming solar radiation

105 (insolation)? (2) How did diatom *sed*aDNA richness change over time?

106

2 Materials and Methods

107

2.1 Study site

108

109   The sediment core SO201-2-12KL was collected from the Kamchatka Strait near

110 Kronotskii Peninsula at the eastern continental slope of Kamchatka where the shelf area is very

111 narrow (Fig. 1). The study area is influenced by water masses transported via the East Kamchatka

112 Current, which brings nutrient-rich waters from the Bering Sea to the subarctic North Pacific

113 Ocean (Stabeno et al., 1999) and by the Alaskan Stream, which transports water masses from the

114 Gulf of Alaska along the Aleutian Arc and water from the wind-driven, cyclonic western subarctic

115 gyre (Nagano et al., 2016; Stabeno & Reed, 1994). As evaporation is lower than precipitation and

116 runoff from Kamchatka, the water column is characterized by a stable halocline (Gebhardt et al.,

117 2008). Modern sea-surface temperatures in the area are about 1 °C in winter and range between 6

118 and 10 °C in summer (Riethdorf et al., 2013a) with winter sea-ice formation only along the coast

119 of Kamchatka (Matul' et al., 2015), but is influenced by drifting sea ice (Polyakova, 2007).

120

121

Figure 1. Map showing the study area with surface current patterns (EKC = East Kamchatka
Current, AS = Alaskan Stream, ANSC = Aleutian North Slope Current; BSC = Bering Sea Current)
indicated by gray arrows and the coring site SO201-2-12KL marked by a yellow dot. The white
dashed line represents median sea-ice extent in March between 1981 and 2010 (Fetterer et al.,
2017). The map was produced with Ocean Data View (Schlitzer, 2002).

127

128   2.2 Sample material

129   Sediment material was retrieved with a piston corer (SO201-2-12KL) during RV Sonne
130   cruise SO-201 (KALMAR) in (Max et al., 2012). The sediment core is 9.05 m long and mostly
131   composed of sandy-silty-clayey mud. We here rely on the chronostratography established by (Max
132   et al., 2012). Core material was stored at 4 °C since retrieval. Samples for ancient DNA analyses
133   were collected in 2018 at GEOMAR, Kiel, in a laboratory devoid of any molecular biology work.
134   To avoid contamination of the samples with modern DNA, sampling was performed from the
135   oldest to the youngest samples while wearing a plastic coverall, face mask, hair net. Gloves were
136   changed between each sample. The treatment of the equipment and the sampling procedure for
137   ancient DNA analyses followed the protocol for non-frozen sediment cores explained in Epp et al.
138   (2019).

139

2.3. DNA extraction and concentration

The DNA extractions, PCR setups and reaction conditions were carried out in a dedicated laboratory for ancient DNA at AWI Potsdam, while PCRs and downstream preparations for sequencing were carried out in the genetics laboratories located in another building. Total DNA was extracted using the DNeasy PowerMax Soil kit (Qiagen, Hilden, Germany) as described in Zimmermann et al. (2017) from 63 samples (2–4 ml sediment). Each extraction batch contained up to 9 samples and one negative control (in total 7 negative controls). Subsequently, we measured the total DNA concentration on a Qubit 4.0 fluorometer (Invitrogen, Carlsbad, CA, USA) using the Qubit dsDNA BR Assay Kit (Invitrogen, Carlsbad, CA, USA). We concentrated for each sample 600 µl of the extracted DNA using the GeneJET PCR Purification KIT (Thermo Scientific, Carlsbad, CA, USA) and eluted twice with 15 µl elution buffer to retain a final volume of ~30 µl. The DNA concentration was measured again and the DNA was diluted to 3 ng/µl. The DNA extracts and aliquots were stored at -20 °C.

153

2.4. *Sed*aDNA metabarcoding

SedaDNA metabarcoding was carried out using the rbcl_76 marker which was designed for both marine and freshwater species (Stoof-Leichsenring et al., 2012). Amplifications were carried out using the primers Diat_rbcL_705F (AACAGGTGAAGTTAAAGGTTCATAYTT) and Diat_rbcL_808R (TGTAACCCATAACTAAATCGATCAT), which were tagged for parallel sequencing (Binladen et al., 2007) as described in Dulias et al. (2017) and Huang et al. (2020). The PCR reaction mixes and conditions were prepared according to the adjusted protocol for tagged Diat_rbcL_705F and Diat_rbcL_808R primers as described in Dulias et al. (2017) with the exception that 3 µl DNA (DNA concentration 3 ng/µl) was used as a template. PCRs were carried out under the following conditions: 5 minutes at 94 °C (initial denaturation), then 50 cycles at 94 °C (denaturation), 49 °C (annealing) and 68 °C (elongation) and a final elongation step at 72 °C for 5 minutes. Each PCR batch was composed of one extraction batch (9 samples and the corresponding extraction negative control) and a PCR negative control. Furthermore, each PCR batch was subjected to three independent PCRs, with distinct primer-tag combinations on different

168   days. PCR success was checked with gel-electrophoresis. Subsequently, the PCR products
169   including all negative controls were purified using the MinElute purification Kit (Qiagen, Hilden,
170   Germany). The DNA concentrations of the PCR products were measured again with the Qubit
171   dsDNA BR Assay Kit and mixed in equal concentrations. As negative controls were below
172   detection limit, 10 µl for negative controls were added to the sample pool. The sample pool was
173   sent to Fasteris SA sequencing service (Switzerland) who carried out library preparation with the
174   Mid Output kit v 2 according to the Fasteris Metafast protocol and sequencing (2 x 150 bp, paired-
175   end) on the Illumina NextSeq 500 platform (Illumina Inc., San Diego, CA, USA). The sequences
176   are deposited at Dryad (Zimmermann et al., 2020a, 2020b).

177

178   2.5 Bioinformatic processing

179   The sequence reads were processed, filtered and assigned a taxonomic name according to
180   the NCBI taxonomy using the OBITools package (Boyer et al., 2016) with the same bioinformatics
181   parameter settings as described in (Dulias et al., 2017). Taxonomic assignment was applied via the
182   EMBL nucleotide reference database (EMBL release 138 from November 2018 (Kanz et al.,
183   2005)) using a least common ancestor approach implemented in OBITools (Table S1). The
184   resulting table was combined with samples sequenced on a previous run (Zimmermann et al.,
185   2020). Then, further denoising was carried out on the combined dataset using R v. 3.6.0 (R Core
186   Team, 2018): PCR and sequencing errors are known to inflate diversity estimates, especially with
187   ancient DNA, hence we kept only those amplicon sequence variants (ASVs) that (1) were assigned
188   a taxonomic name based on 90-100% similarity to an entry in the reference database, (2) were
189   represented with at least 100 read counts in total and (3) at least 10 read counts per PCR-product,
190   (4) were present at least 3 times among all PCR-products, (5) showed taxonomic resolution at least
191   to phylum level "Bacillariophyta", and (6) were tagged as "internal" by obiclean in less than 50%
192   of the different replicates per sample. After filtering, the PCR replicates of a sample were
193   combined and subjected to rarefaction. We resampled the data based on the minimum number of
194   sequences (8,882 counts) using a custom R script (https://github.com/StefanKruse/R_Rarefaction;
195   Kruse, 2019).

196　　　　The negative controls were mostly clean (Table S2). They contained, on average, 38
197　sequence variants of which 90.4% occurred with only one or two read counts, which can most
198　likely be attributed to tag jumps (Schnell et al., 2015). Only one PCR-product of an extraction
199　negative control contained more reads, which was probably a pipetting mistake during PCR-setup,
200　because the corresponding PCR negative control was clean and the other 2 PCR replicates of this
201　negative control were clean as well.

202

203　　　　2.6 Statistical analysis

204　　　　2.6.1 Composition

205　　　　Constrained hierarchical clustering (CONISS; Grimm, 1987) was applied in which clusters
206　were constrained stratigraphically by sample depth with the *chclust*-function from the R package
207　"rioja" v. 0.9-21 (Juggins, 2012). Subsequently we used the bstick-function from the "vegan"
208　package v. 2.5-6 (Oksanen et al., 2011) to compare the dispersion of the computed classification
209　against the dispersion of a broken stick model in order to assess the number of significant zones.
210　The stratigraphic diagram was plotted using *strat.plot* from "rioja" and based only on ASVs having
211　proportions of at least 1% in the dataset.

212

213　　　　2.6.2 Environmental variables

214　　　　Environmental variables were retrieved from PANGAEA (Max et al., 2012b, 2012a;
215　Meyer et al., 2016a; Riethdorf et al., 2013b), NGRIP 20-year means of $\delta^{18}O$
216　(http://www.iceandclimate.nbi.ku.dk/data/2010-11-19_GICC05modelext_for_NGRIP.txt)　　and
217　June insolation was calculated after Laskar et al. (2004). Environmental variables were
218　interpolated using the methods described in Reschke et al. (2019). First, the environmental data
219　were transformed using the function *zoo* from the "zoo" package v. 1.8-7 and used in the function
220　*CorIrregTimser*　　　　using　　　　the　　　　package　　　　"corit"　　　　v.　　　　0.0.0.9000
221　(https://github.com/EarthSystemDiagnostics/corit). As environmental data were limited, we
222　focused the multivariate analyses (package "vegan") on the temporal interval from 7.56–16.48 cal
223　kyr BP. ASVs with proportions of at least 1.5% were selected for multivariate statistical analysis.

224   To avoid double-zeros being regarded as similar between samples we used Hellinger

225   transformation on the reduced proportion-based community matrix with decostand from "vegan".

226   To test for linear dependencies of the environmental variables we ran a constrained

227   correspondence analysis (CCA) and calculated the variance inflation factor (VIF). Furthermore,

228   we applied forward selection using ordistep for stepwise extension of the regression model and

229   performed a permutation test to keep variables that significantly explain some of the variance of

230   the community matrix. Subsequently, we tested the chosen variables with conditional variables for

231   their unique explained variance as forward selection depends on the order by which the variables

232   were put into the model.

233

234   2.6.3 Taxonomic richness and beta-diversity

235   Richness, the number of ASVs, was calculated as a measure of taxonomic alpha-diversity

236   using the *estimateD* function from the iNEXT package v. 2.0.20 (Hsieh et al., 2016), which

237   allowed rarefaction analysis for both centric and pennate diatom ASVs in parallel. Rarefied

238   richness was tested for correlations with interpolated environmental variables using *rcorr* from the

239   package "Hmisc" v. 4.4-0 (Harrell Jr, 2020) with the method "Pearson". Taxonomic beta-diversity

240   was calculated using the *betapart.core* and *beta.pair* functions of the "betapart" v. 1.5.1 package

241   (Baselga & Orme, 2012), which allowed the split of pair-wise Jaccard dissimilarities into

242   nestedness (sample composition is a subset of the previous sample composition) and turnover

243   fractions (taxonomic replacement from one sample to the next). All analyses were carried out using

244   R v. 3.6.0 (R Core Team, 2018).

245

246   **3 Results**

247   A total of 13,584,296 reads were assigned to 3,038 amplicon sequence variants (ASVs) at

248   90–100% similarity to reference sequences. Of these, 2,191 ASVs were specific for diatoms and

249   comprised 11,746,154 reads. After further filtering, 11,114,776 reads remained assigned to 232

250   ASVs, which amounts to 94.6% of all reads assigned to diatoms. Of these, 47% are resolved to

251   species level and 38% to genus level. The lowest number of diatom read counts (8,882 counts)

252 was detected in the sample at 7.885 m depth (18.0 cal kyr BP) while the highest number (914,117

253 counts) was detected in the sample at 3.0 m (11.1 cal kyr BP). The majority of diatom-derived

254 reads were assigned to centric diatoms (92.7%), while 7.3% of reads were assigned to pennate

255 diatoms. The sequence variants were assigned to 25 different families, of which Bacillariaceae (68

256 ASVs), Chaetocerotaceae (40 ASVs), Naviculaceae (18 ASVs) and Thalassiosiraceae (54 ASVs)

257 encompassed the majority of the 231 ASVs that remained after filtering and rarefaction.

258 3.1 Diatom *sed*aDNA composition

259 Throughout the past 19.9 cal kyr BP the sedaDNA composition of the 63 samples is

260 dominated by ASVs assigned to cold-water and sea ice-associated species, such as *Bacterosira*

261 sp., *Nitzschia* (cf.) *frigida*, *Porosira* sp., *Thalassiosira antarctica* and *T. nordenskioeldii*.

262 Dominant ASVs are assigned to centric diatoms of the genera *Chaetoceros*, *Thalassiosira*,

263 *Porosira* and *Skeletonema*.

264 The proportions of ASVs assigned to pennate diatoms per sample ranges between a

265 minimum of 1.4% (2.36 cal kyr BP) and a maximum of 15.1% (19.9 cal kyr BP). Pennate diatoms,

266 predominantly pennate, raphid diatoms, have highest proportions during the end of the LGM

267 (10.9%) and early deglacial (Heinrich Stadial 1 (HS1) (9.8%) and Bølling/Allerød (9%)). Their

268 mean proportions decrease continuously until the Mid Holocene (4.7%), but increase again in the

269 Late Holocene (5.5%) (Fig. 2).

270 Constrained hierarchical clustering combined with the broken stick model suggested

271 division into three stratigraphic zones that are consistent with typical climatic phases: the late

272 glacial phase comprising samples dated to 19.91–15.26 cal kyr BP, the deglacial transition phase

273 comprising samples dated to 14.95–10.73 cal kyr BP and the Holocene phase comprising samples

274 dated to 10.43–1.08 cal kyr BP. We therefore used these phases for the description of the *sed*aDNA

275 record.

276 The glacial phase comprises several ASVs assigned to *Thalassiosira* which account for

277 about 30–70% of the composition, *Porosira* (9.6–29.2%), *Chaetoceros* cf. *contortus* 1 SEH 2013

278 ASV 980 (8.7–9.6%), *Attheya* ASV 58 (0.4–6.8%), *Actinocyclus* 1 MPA-2013 (0.9–5.1 %), and

279 *Chaetoceros socialis* ASV 1280 (0.8–4.7%). Among pennate diatoms, ASVs assigned to
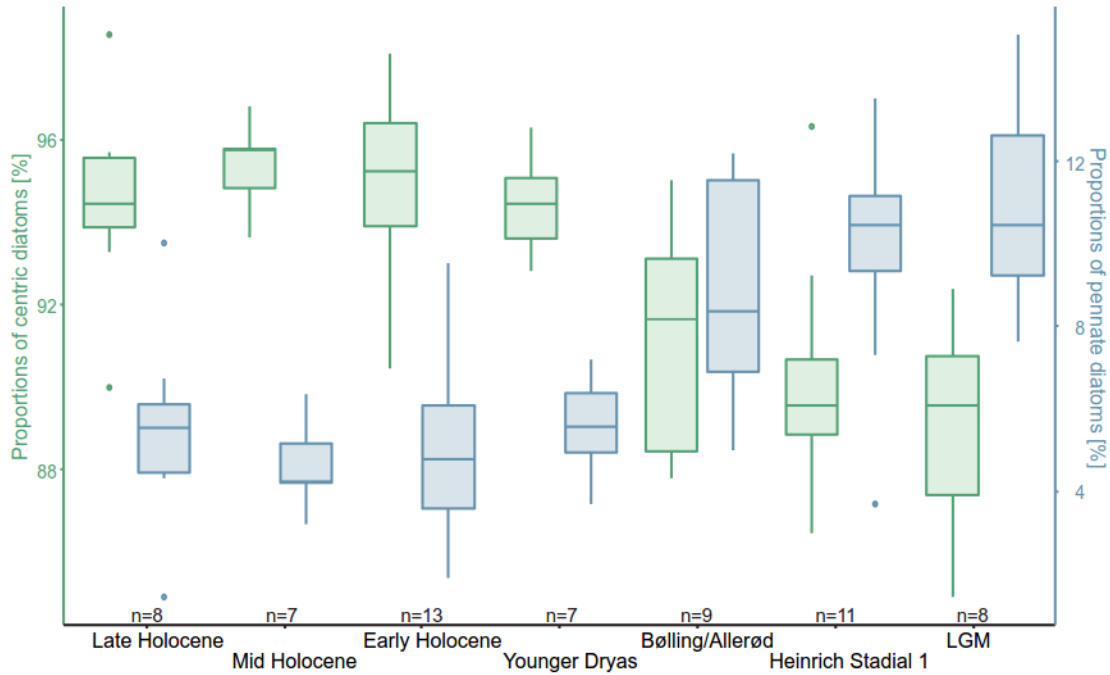
280   *Bacillaria* sp. ASV 139 (0.2–2.7%), *Navicula ramosissima* ASV 1651 (0–2.5%), and several

281   *Nitzschia* ASVs have notable proportions.

282   Although the deglacial phase encompasses climatically very different phases,

283   Cymatosiraceae (0.02–0.7%) and *Leptocylindrus minimus* (0–1.4%) ASVs are mostly restricted to

284   this zone. With the onset of this zone the proportions of most pennate diatoms as well as

285   *Thalassiosira nordenskioeldii* ASV 2697 (mostly <0.1%) decrease. The Bølling/Allerød phase

286   contains ASVs that have their peak proportions during this phase such as *Paralia* (0.6–16.8%) and

287   *Thalassiosira* sp. 15BOF (0–1.2%). While *Thalassiosira angulata* (0.3–5.2%) and *Nitzschia* cf.

288   *frigida* ASVs 1763 and 1764 (1.3–4.8%) increase, *Chaetoceros socialis* ASV 1280 (0–1.4%) and

289   *Minidiscus trioculatus* (0–0.8%) show a marked drop during this phase. During the Younger

290   Dryas, some ASVs that decreased during the Bølling/Allerød, increase again, such as *Chaetoceros*

291   *socialis* ASV 1280 (3–5%), *Thalassiosira* sp. ASV 2241 (2.6–7.4%) and *Attheya* ASV 58 (0–

292   5.7%).

293   The Holocene phase is marked by the reduction and sporadic presence of several ASVs

294   assigned to pennate diatoms, yet increased but highly variable proportions of *Haslea avium* (0.02–

295   4%). Predominatly, the Holocene is composed of sequence types assigned to the genera

296   *Chaetoceros* and *Thalassiosira* as well as *Porosira* (4.4–33.9%) and *Skeletonema* ASV 2155 (0.3-
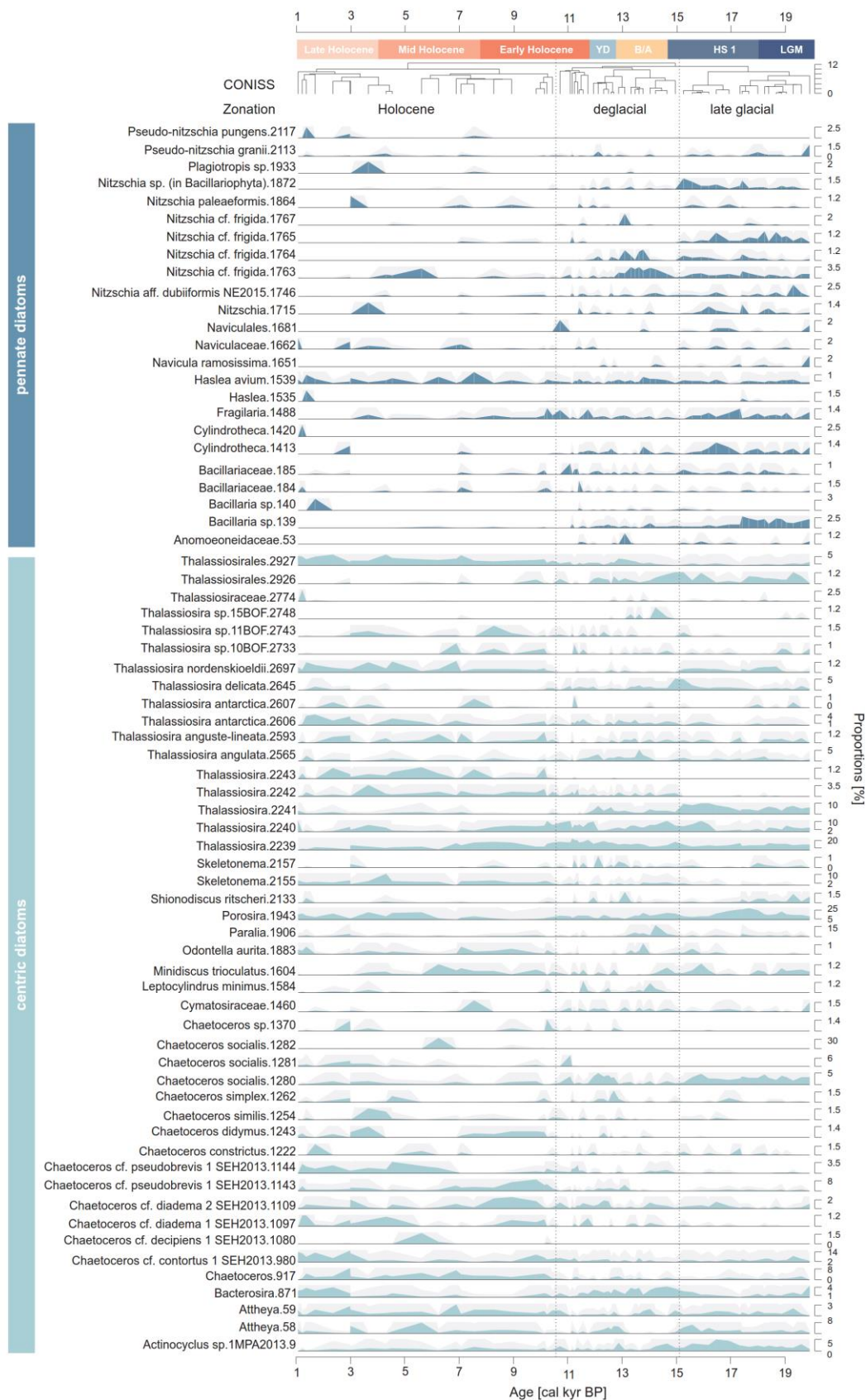
297   10.2%).

298

299

300   **Figure 2**: Proportions of amplicon sequence variants assigned to centric diatoms (red) and

301   pennate diatoms (blue) during the glacial/interglacial transition over of the past 19.9 cal kyr BP.

302

304 **Figure 3:** Stratigraphic diagram showing the proportions of the assigned amplicon sequence
305 variants for each sample through time. Only sequence variants with more than 1% proportion in
306 one or more samples are shown. If not indicated otherwise, the scales of proportions start with 0%.
307 Centric diatoms are marked in light blue, while pennate diatoms are marked in dark blue, 5x
308 exaggeration is shown in gray. The horizontal, dotted lines mark the boundaries of the three
309 CONISS based stratigraphic zones. The CONISS dendrogram and the total sum of squares are
310 given on the right side.

311

312   3.2 Relationship of diatom *sed*aDNA composition with environmental variables

313   We used multivariate statistics to determine to what degree abiotic factors have an effect
314 on the *sed*aDNA composition. Based on variance inflation factors (VIFs) exceeding 10 and thus
315 collinearity with other variables, we stepwise excluded UK'$_{37}$-based SSTs, NGRIP δ^{18}O and the
316 BIT-index (branched and isoprenoid tetraether index, measuring the relative input of terrestrial
317 and marine glycerol dialkyl glycerol teatraethers (GDGTs)) from the set of variables. June
318 insolation, the sea-ice proxy IP$_{25}$ and foraminiferal, ice-volume corrected δ^{18}O (salinity proxy)
319 displayed VIF values between 1.003 and 1.009 suggesting low levels of collinearity between each
320 other. Decomposition of total variance (0.09383) showed that 33.9% of the variance is explained
321 by the model containing the three explanatory variables (adjusted R^2=0.321). RDA axis 1 captures
322 22.6% of the variance, while RDA axis 2 captures 11.3%. June insolation is highly correlated with
323 RDA axis 1 (Table 1). Samples located in the right quadrants of the triplot are characterized by
324 high June insolation and mostly centric diatoms of the genera *Chaetoceros*, *Thalassiosira* and
325 *Skeletonema*. While the upper left quadrant is characterized by high concentrations of the sea-ice
326 biomarker IP$_{25}$, the lower left quadrant is characterized by heavier δ^{18}O$_{ivc-sw}$. Especially in the
327 genus *Chaetoceros*, our dataset shows several ASVs assigned to the same species. The RDA triplot
328 shows, for example, that *Chaetoceros socialis* ASV 1280 is located in the upper left quadrant
329 which is associated with late glacial samples and IP$_{25}$ whereas *Chaetoceros socialis* ASV 1281 is
330 located in the lower right quadrant which is associated with Early Holocene samples of the
331 deglacial stratigraphic zone and high June insolation (Fig. 4). A second example is shown in the
332 RDA triplot for two ASVs assigned to *Chaetoceros* cf. *pseudobrevis* 1 SHE-2013 with closest
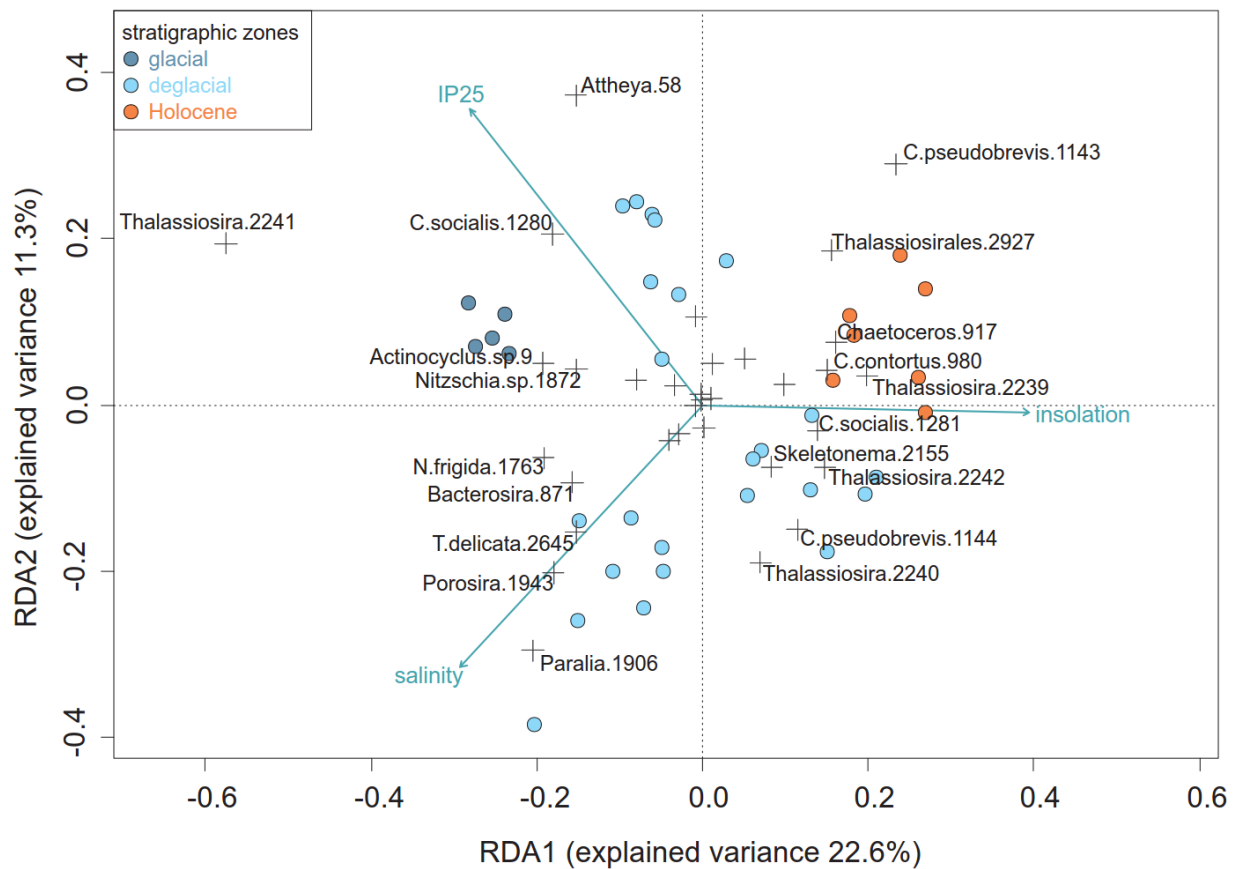
333   match to the same GenBank accession number (KC985654). While ASV 1143 (98% match with

334   reference) is located in the upper right quadrant and has its highest proportions during the Early

335   Holocene and is strongly reduced since the Mid Holocene (Fig. 3), the proportions of ASV 1144

336 (100% match with reference) increase in the early Mid Holocene and remain on a rather similar

337 level until the Late Holocene.

338

339 **Table 1:** Variation partitioning for the final set of explanatory variables with adjusted R^2 and p-

340 values for the single and the individual fractions (conditional variance) which remain after

341 eliminating the effects of the remaining explanatory variables.

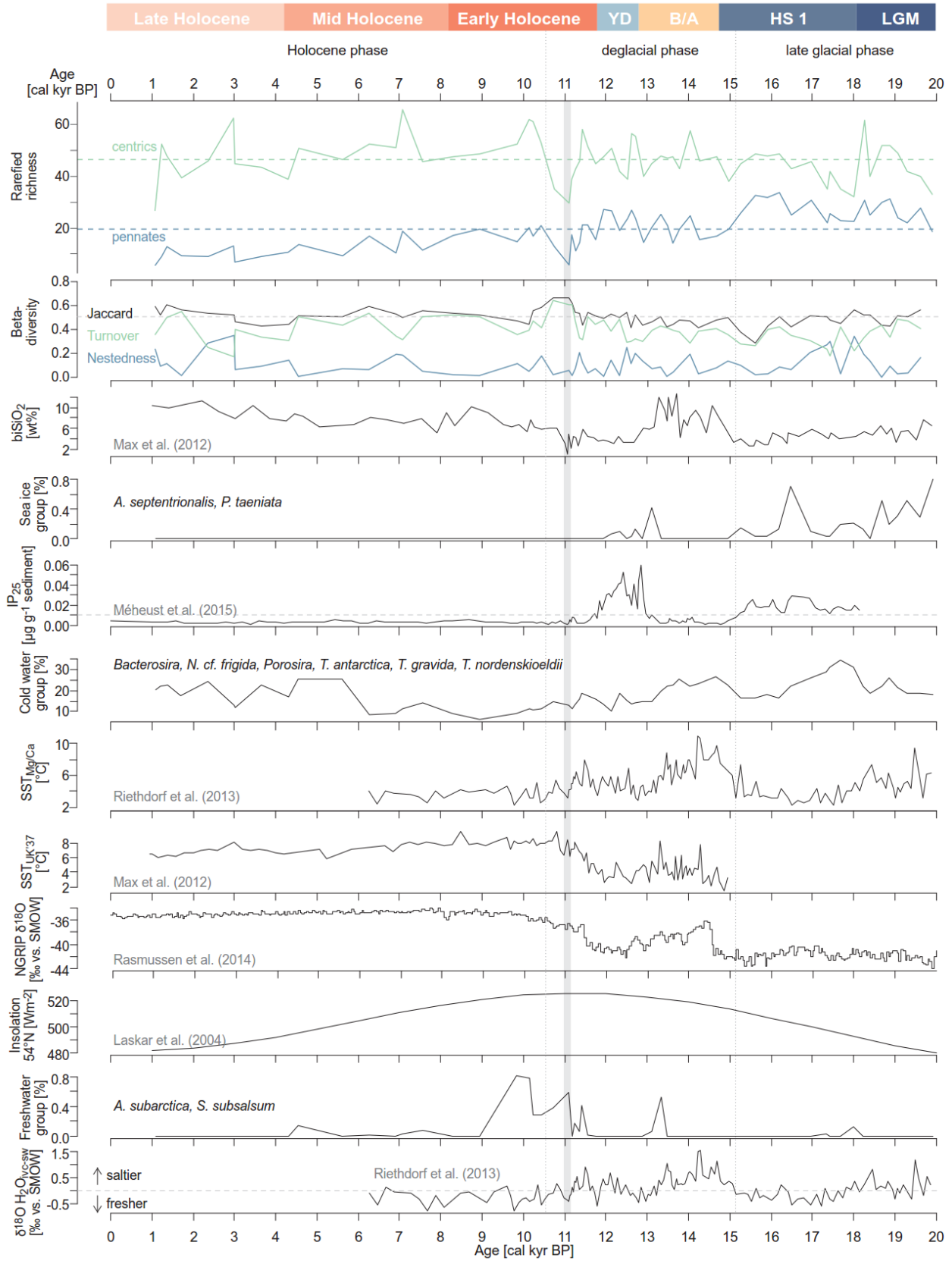|		single		conditional	
	variance	adj. R^2	p-value	adj. R^2	p-value
June insolation	0.0116	0.108	0.002	0.040	0.001
IP_{25}	0.0119	0.104	0.002	0.089	0.001
salinity	0.0113	0.099	0.001	0.023	0.01

342

Figure 4: RDA triplot showing the abbreviated names of the 20 most explaining amplicon sequence variants (ASVs) and the vector ends of the most abundant ASVs as a gray plus symbol (+). Samples are marked by colour coded points to the three stratigraphic zones which they represent (dark blue = late glacial, light blue = deglacial, orange = Holocene). Environmental variables are shown by blue vectors.

3.3 Diatom diversity changes

Richness (number of ASVs after rarefaction) was lowest in the youngest sample dated to 1.08 cal kyr BP (37 ASVs) and highest about 18.42 cal kyr BP (106 ASVs) (Fig. 5, Fig. S1). While the median richness among sequences assigned to centric diatoms varies only slightly over the past 19.9 cal kyr BP, the richness of those assigned to pennate diatoms declines almost continuously throughout the record, except for an increase during the Younger Dryas (Fig. S1). The richness of

356   pennate diatom ASVs shows a moderate, positive correlation with IP_{25} (R=0.48, p=0.003), and

357   moderate, negative correlations with June insolation (R=-0.49, p=0.002) and NGRIP $\delta^{18}O$ (R=-

358   0.68, p<0.001). The richness of centric diatoms does not show any significant correlation with

359   environmental variables Table S1).

360   Beta-diversity, which is here used as a measure of dissimilarity between adjacent samples,

361   is moderate overall (median=0.51). There are four strong declines in diatom richness in our record.

362   The first occurred between 18.24 and 18 cal kyr BP and reduced centric diatom ASVs

363   approximately by half (from 62 to 32 ASVs) and pennate ASVs by about a quarter (from 31 to 23

364   ASVs). Slightly elevated values of beta-diversity (Jaccard dissimilarity=0.56) during this time in

365   comparison to the median Jaccard dissimilarity correspond more to nestedness rather than turnover

366   (Fig. 3). The second decline occurred between 15.6 and 14.24 cal kyr BP and affected pennate

367   diatom ASVs (from 33 to 16 ASVs) more than centric ones (from 49 to 38 ASVs). Beta-diversity

368   increases from 15.6 to 14.95 cal kyr BP and then slightly decreases again. The third decline affects

369   both pennate and centric diatoms strongly and started after 11.95 until 11.1 cal kyr BP for pennate

370   (from 27 to 6 ASVs) and after 11.42 until 11.1 cal kyr BP for centric diatom ASVs (from 58 to 30

371   ASVs). Between 11.1 and 10.5 cal kyr BP, the turnover partition of beta-diversity is highest overall

372   throughout the record. This corresponds predominantly to a loss of ASVs in both pennate and

373   centric diatoms at 11.1 cal kyr BP followed by a gain of ASVs at 10.5 cal kyr BP (Fig.5). The

374   fourth decline is detected between the youngest samples from 1.22 and 1.08 cal kyr BP (from 9 to

375   6 pennate ASVs and from 53 to 27 centric ASVs) and shows slightly increased beta-diversity, of

376   which the turnover partition is only slightly higher than the nestedness one.

377

378

379   **Figure 5:** Comparison of rarefied richness (horizontal green dashed line marks median richness

380   of centric diatom ASVs, blue dashed line marks median richness of pennate diatom ASVs), beta-

381   diversity (Jaccard dissimilarity and its partitions into turnover and nestedness) and proportions of

382   diatom *sed*aDNA indicator groups with Mg/Ca-based subsurface SSTs (Riethdorf et al., 2013a),

383   alkenone-based surface SST$_{UK'37}$, biogenic silica (Max et al., 2012), IP$_{25}$ (Méheust et al., 2015),

384   stable oxygen isotopes from Greenland ice cores (NGRIP δ^{18}O; Rasmussen et al., 2014), June

385   insolation calculated after Laskar et al. (2004) and sea subsurface salinity appoximation (δ^{18}O$_{ivc-}$

386    $_{sw}$; Riethdorf et al., 2013a). The vertical dotted lines mark the stratigraphic zonation. The shaded

387   vertical area highlights the sample at ~11.1 cal kyr BP.

388

389   **4 Discussion**

390   4.1 General relationship between diatom *sed*aDNA composition and environmental

391   change

392   4.1.1 Late glacial phase (19.9–15.26 cal kyr BP)

393   The diatom *sed*aDNA composition during the late glacial phase reflects sea ice as a key

394   variable shaping the past diatom communities. The presence of winter sea ice is indicated by

395   sequences assigned to sea ice-associated species such as the colony-forming pennate diatoms

396   *Pauliella taeniata* (Grunow) Round & Basson (Lovejoy et al., 2002; Syvertsen, 1991) and

397   *Nitzschia* cf. *frigida* (Grunow) (Hasle & Heimdal, 1998), or the epiphytic living *Attheya*

398   *septentrionalis* (Østrup) R.M.Crawford (von Quillfeldt, 1997). These species are frequently

399   detected in modern surveys of sea ice (Limoges et al., 2018; Lovejoy et al., 2002; Poulin et al.,

400   2011; von Quillfeldt, 2000), but can be absent or only sporadically found in surface sediments due

401   to degradation during sinking through the water column (Limoges et al., 2018; Lopes et al., 2006).

402   Here, the *sed*aDNA has an advantage over morphological data and can complement the picture we

403   perceive of the past. Winter sea-ice conditions with ice-free summers were also reconstructed

404   based on the sea-ice biomarker IP$_{25}$ and abundant *Fragilariopsis cylindrus* and *F. oceanica* in local

405   microfossil assemblages (Max et al., 2012; Méheust et al., 2016; Smirnova et al., 2015). Low

406   proportions of sequences assigned to the productive genus *Chaetoceros* (Lopes et al., 2006) in our

407 record could reflect overall low productivity as also suggested by low biogenic silica (Max et al.,

408 2012) and low abundance of diatom microfossils during this phase (Smirnova et al., 2015).

409   The high share of sequences assigned to *Bacterosira* (probably *B. bathyomphala*),

410 *Thalassiosira nordenskioeldii*, *T. antarctica* and *Porosira* (probably *P. glacialis*) points to ice-

411 free, but cool, summers. These cold-water species are often found along the winter ice edge in the

412 Bering and Okhotsk Seas and in coastal areas of Kamchatka (Ren et al., 2014), although the neritic

413 species *Bacterosira bathyomphala* could also be associated with shallow slope depths down to 500

414 m in the Sea of Okhotsk (Ren et al., 2014; Sancetta, 1982). In the subarctic North Pacific and

415 adjacent seas, these species achieve maximum abundances where summer SSTs remain between

416 5 to 8 °C, but they can generally be found where summer SSTs remain below 12.5 °C (Ren et al.,

417 2014). This is well within the range of previous reconstructions carried out on this sediment core

418 indicating summer SSTs of about 8 to 9.5 °C during this phase (Meyer et al., 2016b). Late glacial

419 diatom microfossil data of this core are characterized by dominance of the *Thalassiosira trifulta*

420 and *Actinocyclus curvatulus* group. While our *sed*aDNA reveals much more complexity in the

421 diatom assemblages during this time, our method is still restricted by the incompleteness of the

422 reference database, as, for example, *T. trifulta* and *A. curvatulus* are not available and are

423 potentially only resolved to genus level in our record. Still, *Actinocyclus* sp. 1 MPA-2013 displays

424 higher proportions during the late glacial phase in comparison to the deglacial and Holocene

425 phases, which is in agreement with Smirnova et al. (2015) as well as with microfossil records from

426 Bowers Ridge and the western subarctic gyre (Katsuki & Takahashi, 2005).

427   Sequences assigned to pennate, raphid diatoms have the highest proportions until

428 approximately 15.7 cal kyr BP, which may be linked to bottom ice communities (Caissie et al.,

429 2010). Even though pennate diatoms are often poorly preserved as microfossils in sediments

430 (Limoges et al., 2018), they are usually dominant in sea ice (Poulin et al., 2011; von Quillfeldt,

431 2000). The benthic lifestyle, to which pennate diatoms are adapted to, includes the excretion of

432 exopolymers via the raphe, which facilitate their attachment to surfaces and enables them to

433 actively move along surfaces such as ice (Olsen et al., 2019; Round et al., 1990). As summer

434 insolation is an important driver for SSTs in the subarctic North Pacific (Harada et al., 2014), it is

435 conceivable that the low summer insolation during this time (Laskar et al., 2004) promoted pennate

436 diatoms due to a long duration of sea-ice coverage with only a short summer. Short-term summers

437 have also been reconstructed during this phase in the Bering Sea where sea ice was estimated to

438   have covered most of the Bering Sea for more than six months (Caissie et al., 2010; Méheust et
439   al., 2016).

440

441   4.1.2 Deglacial transition phase (14.95–10.73 cal kyr BP)

442   The *sed*aDNA composition of samples dated to the Bølling/Allerød phase (14.7–12.7 cal
443   kyr BP) can likely be related to increased local subsurface salinity conditions in comparison to the
444   glacial phase as implied by an enrichment of foraminifera-derived stable oxygen isotopes
445   ($\delta^{18}O_{ivc-sw}$ (Riethdorf et al., 2013a)). Peak proportions of sequences assigned to *Paralia* (*sulcata*)
446   up to ~15% coincide with increasing subsurface salinities (positive $\delta^{18}O_{ivc-sw}$) during this phase.
447   *Paralia sulcata* (Ehrenberg) Cleve is a coastal species, which is a common part of benthic
448   communities and increased abundance is often recorded in areas of upwelling (Abrantes, 1988;
449   McQuoid & Nordberg, 2003; Stabell, 1986), or where the water column is less stable and subject
450   to strong wind-driven or tidal mixing (McQuoid & Nordberg, 2003).

451   Sequences assigned to *Thalassiosira delicata*, the cold-water indicator *Porosira*, and
452   *Bacterosira*, but also to the sea-ice associated *Nitzschia* cf. *frigida* suggest a cold-water
453   environment with frequent influence of sea ice despite recorded increases of SSTs by about 3–
454   5 °C (Max, Riethdorf, Tiedemann, Smirnova, Lembke-Jene, et al., 2012; Riethdorf et al., 2013a).
455   Such SSTs are still in the growth range of *B. bathyomphala* and *P. glacialis* which occur in the
456   Bering and Okhotsk Seas in regions with summer SSTs between 5 and 12.5 °C (Ren et al., 2014).
457   These species also occur in the marginal ice zone, where sea-ice concentration varies between 15
458   and 80%, and achieve high abundances during the spring bloom (Hasle, 1990). Hence, proportions
459   of sequences assigned to *Nitzschia* cf. *frigida* of more than 3% in this phase are not necessarily
460   contradictory. While the absence of IP$_{25}$ suggests ice-free conditions, gravel-sized ice rafted debris
461   at about 13.86 cal kyr BP (560 cm depth; Levitan et al., 2015) point towards the presence of sea
462   ice. As *Nitzschia frigida* is a common inhabitant of landfast ice communities (Medlin & Hasle,
463   1990), a possible explanation could be the occurrence of drifting ice floes, which were transported
464   away from the coast or southward by the East Kamchatka Current, and probably originated from
465   enclosed bights and bays along the eastern coast of Kamchatka (Polyakova, 2007).

466   The diatom *sed*aDNA composition of samples dated to the Younger Dryas (12.7–11.7 cal
467   kyr BP) are characterized by the presence of sea ice-associated ASVs (*Pauliella taeniata*, *Attheya*

468 *septentrionalis, Nitzschia* cf. *frigida*) suggesting winter sea-ice coverage during this time. Sea ice-
469 associated ASVs in combination with a higher richness of pennate diatom ASVs in comparison to
470 the Bølling/Allerød phase are in agreement with sea-ice diatom microfossils detected by Smirnova
471 et al. (2015), high concentrations of the sea-ice biomarker IP$_{25}$ (Méheust et al., 2016) and
472 reconstructed subsurface SSTs between about 2–5 °C with lower seasonal contrasts and a reduced
473 stratification of the mixed layer (Riethdorf et al., 2013a).

474 Increased proportions of *Chaetoceros socialis* (ASV 1280) are characteristic in this phase
475 and show comparable proportions with regard to the late glacial phase. This matches increasing
476 proportions of *Chaetoceros* spp. detected in the microfossil record during this phase (Smirnova et
477 al., 2015). *Chaetoceros socialis* is often dominant in coastal areas with sparse to no sea ice in the
478 Greenland North Water Polynya, where it blooms in late summer; however, it can also achieve
479 substantial abundances in sea ice (Booth et al., 2002; von Quillfeldt, 1997). We therefore assume
480 that this ASV is derived from a lineage adapted to sea ice or marginal ice zone conditions and
481 might actually represent the novel described *C. gelidus* Chamnansinp, Y.Li, Lundholm &
482 Moestrup (Chamnansinp et al., 2013).

483 The composition of samples dated to the onset of the Preboreal (11.7–10.73 cal kyr BP)
484 are marked by a decrease in sequences assigned to cold-water diatoms and highest proportions of
485 sequences assigned to freshwater species throughout the record. From about 11.2 cal kyr BP
486 onwards, sequences assigned to *Skeletonema subsalsum* (Cleve-Euler) Bethge and *Aulacoseira*
487 *subarctica* (Otto Müller) E.Y.Haworth increase strongly. *Skeletonema subsalsum* can be found in
488 rivers, estuaries and coastal areas (Hasle & Evensen, 1975) while *A. subarctica* is a freshwater
489 species occurring in rivers and turbulent, cool lakes on Kamchatka (Lepskaya et al., 2010). Their
490 increased proportions in the *sed*aDNA record suggest an increased runoff from Kamchatka and
491 possibly fresher sea-surface conditions. The timing coincides with the post-glacial opening of the
492 Bering Strait (Jakobsson et al., 2017) and is marked by a high June insolation (Laskar et al., 2004).
493 Fresher subsurface conditions are also indicated by peaks of lighter $\delta^{18}O_{ivc-sw}$ in this core
494 (Gorbarenko et al., 2019; Riethdorf et al., 2013a). Even though terrestrial lipid biomarkers and
495 titanium/calcium records of this core suggest low terrestrial input, the sum of terrestrial soil derived
496 branched GDGTs peaks during this time (Meyer et al., 2016b, 2017) and might also point towards
497 increased runoff from Kamchatka.

498

499   4.1.3 Holocene phase (10.43–1.08 cal kyr BP)

500   The s*ed*aDNA composition of the Early to Mid Holocene is characterized by reduced

501   proportions of sequences assigned to cold-water species and correlate with high June insolation

502   between ~11 and 6 cal kyr BP (Laskar et al., 2004). The timing fits well into the range of the

503   Holocene Thermal Maximum between ~10 and 8 cal kyr BP (Meyer et al., 2017), with maximum

504   SSTs ranging from 6–11 °C (SST$_{UK'37}$) as reconstructed by (Max et al., 2012) to 10–11 °C

505   (SST$_{TEXL86}$ August temperatures of Meyer et al., 2016b). During this phase, the proportions of

506   sequences assigned to centric diatoms, especially of the genera *Chaetoceros*, *Thalassiosira* and

507   *Skeletonema*, increase at the expense of sequences assigned to pennate diatoms.

508   High proportions of *Chaetoceros* are indicative of high productivity, which is supported

509   by increasing biogenic opal (Max et al., 2012; Riethdorf et al., 2013a) and high diatom microfossil

510   abundances (Smirnova et al., 2015). Sequences assigned as freshwater diatoms and negative

511    $\delta^{18}O_{ivc-sw}$ values indicate long-term relatively fresh subsurface conditions (Riethdorf et al., 2013a).

512   From about 6–1 cal kyr BP, increasing proportions of cold-water diatom ASVs reflect

513   cooling, which is in agreement with the climate development recorded in the NGRIP Greenland

514   ice core record (Rasmussen et al., 2014), reconstructed SSTs (Max et al., 2012; Meyer et al., 2016b,

515   2017; Riethdorf et al., 2013a) and the advance of glaciers on Kamchatka (between 4.5 and 3.5 cal

516   kyr BP) (Brooks et al., 2015). A drop in cold-water diatoms at ~3 cal kyr BP, suggests a short-

517   term interruption of this phase of cooling, which is synchronous with a short-term increase of

518   SST$_{UK'37}$ (Max et al., 2012).

519   An increase of sequences assigned to pennate diatoms in the Late Holocene and high

520   proportions of cold-water diatom ASVs including the ice-associated *Nitzschia* cf. *frigida* suggest

521   cooling and potentially an increasing influence of winter sea ice or at least drifting ice floes in the

522   region. In support of this, grain-size analyses of this core suggest increased presence of potentially

523   ice-rafted material (Levitan et al., 2015) and after 6 cal kyr BP the microfossil assemblage contains

524   sea ice-associated species (Smirnova et al., 2015), whereas the sea-ice biomarker IP$_{25}$ suggests ice-

525   free conditions (Méheust et al., 2016). Thus, *sed*aDNA has the potential to complement our

526   understanding of past sea-ice distribution.

527   A second sequence variant of *Chaetoceros socialis* (ASV 1281) is linked with Holocene

528   samples and suggests that different ASV are potentially derived from different lineages adapted to

529   different growth conditions (Hamsher et al., 2013). In several cases, different ASVs which were

530   assigned to the same species co-occurred while a few showed patterns consistent with changes in

531   environmental conditions. Such co-occurrence of several ASVs could arise due to the degraded

532   state of ancient DNA introducing erroneous nucleotides during PCR (Hofreiter et al., 2001), but it

533   is also in agreement with the ecological hypothesis that genetic variation allows species to quickly

534   adapt to changing environmental conditions (Godhe & Rynearson, 2017). The application of

535   ASVs, in comparison to clustering into operational taxonomic units, thus has the advantage of

536   revealing (pseudo-)cryptic species or ecotypes and should be considered more in biogeographic

537   surveys.

538

539   4.2 Changes in diatom *sed*aDNA richness and the relationship with environmental

540   changes

541   Richness of pennate diatom ASVs was higher during phases of strong Northern

542   Hemisphere cooling, namely the late LGM, Heinrich Stadial 1 and the Younger Dryas and is

543   significantly positively correlated with sea ice and significantly negatively correlated with June

544   insolation and Northern Hemisphere temperatures. This points towards sea ice as a facilitating

545   factor for pennate diatoms with regard to alpha-diversity in the subarctic NW Pacific. The negative

546   correlation of pennate diatom richness with June insolation and temperatures in comparison to

547   centric diatom richness might be related to the higher sensitivity of pennate diatoms to ultraviolet

548   light in the absence of a thick sea-ice cover, whereas centric diatoms have developed strategies to

549   prevent damage to their photosystems (Enberg et al., 2015).

550   A strong decline of richness accompanied by increased beta-diversity occurred during the

551   Preboreal phase of the Early Holocene around 11.1 cal kyr BP and could be attributed

552   predominantly to turnover by loss of ASVs until 11.1 cal kyr BP and replacement by different

553   ASVs towards 10.5 cal kyr BP. This decline of richness occurs simultaneously with a sharp drop

554   in biogenic opal, suggesting strongly reduced productivity of siliceous organisms such as diatoms

555   (Max, Riethdorf, Tiedemann, Smirnova, Lembke-Jene, et al., 2012). This interval is characterized

556   by a peak in summer insolation, rising SSTs (Max et al., 2012) and strong sea-level rise which

557   culminated in the opening of the Bering Strait (Jakobsson et al., 2017). A sharp increase in

558   proportions of the freshwater group and foraminiferal stable oxygen isotopes points towards

559   increased sea-surface freshening, potentially derived from increased runoff from Kamchatka

560   (Gorbarenko et al., 2019; Riethdorf et al., 2013a) as suggested by a peak in terrestrial lipid

561   biomarkers around 11.2 cal kyr BP (Meyer et al., 2016b, 2017). Fresher surface conditions could

562   have resulted in enhanced vertical stratification limiting the mixing of nutrients from deeper water

563   masses toward the euphotic zone and thus restricting primary productivity, manifested as a sharp

564   drop of biogenic silica during this time (Max et al., 2012).

565   To what extent changes in the diversity and composition of past diatom assemblages

566   affected the past organismal community at the ecosystem level remains to be revealed. Diatoms

567   have been shown to impact marine plankton structure by biotic interactions, for example by

568   competition or selective grazing (Vincent & Bowler, 2020) and exopolymers excreted by sea-ice

569   diatoms have been shown to be hotspots for enhanced bacterial activity (Meiners et al., 2008).

570   Hence, changes might be linked to several trophic levels and could substantially impact marine

571   food-webs and biogeochemical cycling in areas such as the Arctic where food-webs have evolved

572   over millions of years.

573

574   5 Conclusions

575   We present the first diatom-derived *sed*aDNA metabarcoding record of the subarctic NW

576   Pacific, which covers the past 19.9 cal kyr.

577   The dominant components of the diatom *sed*aDNA composition fit well within the

578   framework of reconstructed sea-ice dynamics, SSTs and subsurface salinities over the past

579   millennia. High proportions of sea-ice and cold-water associated diatoms and generally high

580   proportions of pennate diatoms point to sea ice as a main driver of diatom composition during the

581   late glacial phase as well as during the Younger Dryas. A positive correlation of pennate diatom

582   richness with the sea-ice biomarker IP_{25} suggests that an extended winter sea-ice cover during the

583   late glacial and the Younger Dryas potentially acted as a diversifying force.

584   Substantial proportions of *Nitzschia* cf. *frigida* in the absence of the sea-ice proxy IP_{25}

585   during the early deglacial phase point to a continued influence of drifting sea ice. This suggests

586 either that the ecology of *N. frigida* is not completely understood yet, or that our proxy can
587 occasionally be more sensitive to the past presence of sea ice than IP$_{25}$.

588   Unfavorable conditions for pennate diatoms at the start of the Holocene is suggested by
589 decreasing proportions and the negative correlation of pennate diatom richness with June
590 insolation and temperature.

591   The inferred loss of 42% of diatom ASVs at ~11.1 cal kyr BP is accompanied by freshwater
592 diatoms implying the influence of runoff from Kamchatka to the local assemblage. It is likely that
593 the freshwater input resulted in enhanced vertical stratification limiting the mixing of nutrients
594 from deeper water masses toward the euphotic zone and thus restricting primary productivity – a
595 scenario which is supported by near-zero biogenic silica during this time. As modern climate
596 warming is anticipated to increase freshwater input into the Arctic from 11 to 30% by river
597 discharge alone (Nummelin et al., 2016), an enhanced stratification with restricted nutrient supply
598 could have tremendous consequences for the biological carbon pump, biogeochemical cycling and
599 the food-web in the Arctic.

600   Finally, our proxy revealed shifts of potential ecotypes of species from the genus
601 *Chaetoceros,* which is in agreement with the concept that intra-specific variation facilitates an
602 adaptive response to changing environmental conditions and is particularly relevant in high-
603 latitudinal ecosystems. Therefore, marine *sed*aDNA has the potential to answer ecological
604 questions regarding selective or adaptive responses at an intra-specific level where morphological
605 studies might be severely limited.

606

616   the RV Sonne. The KALMAR Project (SO201-2- KALMAR Leg 2) was funded by the Federal

617   German Ministry of Education and Research (BMBF).

618

619   **References**

620   Abrantes, F. (1988). Diatom assemblages as upwelling indicators in surface sediments off Portugal. *Marine*

621   *Geology*, *85*(1), 15–39. https://doi.org/10.1016/0025-3227(88)90082-5

622   Baselga, A., & Orme, C. D. L. (2012). betapart: an R package for the study of beta diversity. *Methods in Ecology*

623   *and Evolution*, *3*(5), 808–812. https://doi.org/10.1111/j.2041-210X.2012.00224.x

624   Binladen, J., Gilbert, M. T. P., Bollback, J. P., Panitz, F., Bendixen, C., Nielsen, R., & Willerslev, E. (2007). The

625   use of coded PCR primers enables high-throughput sequencing of multiple homolog amplification products

626   by 454 parallel sequencing. *PLoS ONE*, *2*(2), e197. https://doi.org/10.1371/journal.pone.0000197

627   Booth, B. C., Larouche, P., Bélanger, S., Klein, B., Amiel, D., & Mei, Z.-P. (2002). Dynamics of *Chaetoceros*

628   *socialis* blooms in the North Water. *Deep Sea Research Part II: Topical Studies in Oceanography*, *49*(22),

629   5003–5025. https://doi.org/10.1016/S0967-0645(02)00175-3

630   Boyer, F., Mercier, C., Bonin, A., Le Bras, Y., Taberlet, P., & Coissac, E. (2016). OBITools: a Unix-inspired

631   software package for DNA metabarcoding. *Molecular Ecology Resources*, *16*, 176–182.

632   https://doi.org/10.1111/1755-0998.12428

633   Brooks, S. J., Diekmann, B., Jones, V. J., & Hammarlund, D. (2015). Holocene environmental change in

634   Kamchatka: A synopsis. *Global and Planetary Change*, *134*, 166–174.

635   https://doi.org/10.1016/j.gloplacha.2015.09.004

636   Caissie, B. E., Brigham-Grette, J., Lawrence, K. T., Herbert, T. D., & Cook, M. S. (2010). Last Glacial Maximum to

637   Holocene sea surface conditions at Umnak Plateau, Bering Sea, as inferred from diatom, alkenone, and

638   stable isotope records. *Paleoceanography*, *25*(1). https://doi.org/10.1029/2008PA001671

639   Chamnansinp, A., Li, Y., Lundholm, N., & Moestrup, Ø. (2013). Global diversity of two widespread, colony-

640   forming diatoms of the marine plankton, *Chaetoceros socialis* (syn. *C. radians*) and *Chaetoceros gelidus*

641   sp. nov. *Journal of Phycology*, *49*(6), 1128–1141. https://doi.org/10.1111/jpy.12121

642   Corinaldesi, C., Beolchini, F., & Dell'anno, A. (2008). Damage and degradation rates of extracellular DNA in

643   marine sediments: implications for the preservation of gene sequences. *Molecular Ecology*, *17*(17), 3939–

644   3951. https://doi.org/10.1111/j.1365-294X.2008.03880.x

645   Coupel, P., Ruiz-Pino, D., Sicre, M. A., Chen, J. F., Lee, S. H., Schiffrine, N., et al. (2015). The impact of

646   freshening on phytoplankton production in the Pacific Arctic Ocean. *Progress in Oceanography*, *131*, 113–

647   125. https://doi.org/10.1016/j.pocean.2014.12.003

648   De Schepper, S., Ray, J. L., Skaar, K. S., Sadatzki, H., Ijaz, U. Z., Stein, R., & Larsen, A. (2019). The potential of

649   sedimentary ancient DNA for reconstructing past sea ice evolution. *The ISME Journal*.

650   https://doi.org/10.1038/s41396-019-0457-1

651   Degerlund, M., Huseby, S., Zingone, A., Sarno, D., & Landfald, B. (2012). Functional diversity in cryptic species of

652   *Chaetoceros socialis* Lauder (Bacillariophyceae). *Journal of Plankton Research*, *34*(5), 416–431.

653   https://doi.org/10.1093/plankt/fbs004

654   Dulias, K., Stoof-Leichsenring, K. R., Pestryakova, L. A., & Herzschuh, U. (2017). Sedimentary DNA versus

655   morphology in the analysis of diatom-environment relationships. *Journal of Paleolimnology*, *57*(1), 51–66.

656   https://doi.org/10.1007/s10933-016-9926-y

657   Enberg, S., Piiparinen, J., Majaneva, M., Vähätalo, A. V., Autio, R., & Rintala, J.-M. (2015). Solar PAR and UVR

658   modify the community composition and photosynthetic activity of sea ice algae. *FEMS Microbiology*

659   *Ecology*, *91*(10). https://doi.org/10.1093/femsec/fiv102

660   Epp, L. S., Zimmermann, H. H., & Stoof-Leichsenring, K. R. (2019). Sampling and Extraction of Ancient DNA

661   from Sediments. In B. Shapiro, A. Barlow, P. D. Heintzman, M. Hofreiter, J. L. A. Paijmans, & A. E. R.

662   Soares (Eds.), *Ancient DNA: Methods and Protocols* (pp. 31–44). New York, NY: Springer New York.

663   https://doi.org/10.1007/978-1-4939-9176-1_5

664   Fetterer, F., Knowles, K., Meier, W. N., Savoie, M., & Windnagel, A. K. (2017). Sea Ice Index, Version 3. Monthly

665   and daily GIS compatible shapefiles of median ice extent [Data set]. NSIDC: National Snow and Ice Data

666   Center. https://doi.org/10.7265/n5k072f8

667   Gebhardt, H., Sarnthein, M., Grootes, P. M., Kiefer, T., Kuehn, H., Schmieder, F., & Röhl, U. (2008). Paleonutrient

668   and productivity records from the subarctic North Pacific for Pleistocene glacial terminations I to V.

669   *Paleoceanography*, *23*(4). https://doi.org/10.1029/2007PA001513

670   Gorbarenko, S., Shi, X., Zou, J., Velivetskaya, T., Artemova, A., Liu, Y., et al. (2019). Evidence of meltwater pulses

671   into the North Pacific over the last 20 ka due to the decay of Kamchatka Glaciers and Cordilleran Ice Sheet.

672   *Global and Planetary Change*, *172*, 33–44. https://doi.org/10.1016/j.gloplacha.2018.09.014

673   Grimm, E. C. (1987). CONISS : A FORTRAN 77 Program for stratigraphically constrained cluster analysis by the

674   method of incremental sum of squares. *Computers and Geosciences*, *13*(I), 13–35.

675   Hamsher, S. E., LeGresley, M. M., Martin, J. L., & Saunders, G. W. (2013). A comparison of morphological and

676   molecular-based surveys to estimate the species richness of *Chaetoceros* and *Thalassiosira*

677   (Bacillariophyta), in the Bay of Fundy. *PLOS ONE*, *8*(10), e73521.

678   https://doi.org/10.1371/journal.pone.0073521

679   Harada, N., Katsuki, K., Nakagawa, M., Matsumoto, A., Seki, O., Addison, J. A., et al. (2014). Holocene sea surface

680   temperature and sea ice extent in the Okhotsk and Bering Seas. *Progress in Oceanography*, *126*, 242–253.

681   https://doi.org/10.1016/j.pocean.2014.04.017

682   Harrell Jr, F. E. (2020). *Hmisc: Harrell Miscellaneous. R package version 4.4-0. https://CRAN.R-*

683   *project.org/package=Hmisc*.

684   Hasle, G. R. (1990). Arctic plankton diatoms: dominant species, biogeography. In L. K. Medlin & J. Priddle, *Polar*

685   *Marine Diatoms* (pp. 53–56). British Antarctic Survey, Natural Environment Research Council.

686   Hasle, G. R., & Evensen, D. L. (1975). Brackish-water and fresh-water species of the diatom genus *Skeletonema*

687   Grev. I. *Skeletonema subsalsum* (A. Cleve) Bethge. *Phycologia*, *14*(4), 283–297.

688   https://doi.org/10.2216/i0031-8884-14-4-283.1

689   Hasle, G. R., & Heimdal, B. R. (1998). The net phytoplankton in Kongsfjorden, Svalbard, July 1988, with general

690   remarks on species composition of Arctic phytoplankton. *Polar Research*, *17*(1), 31–52.

691   https://doi.org/10.3402/polar.v17i1.6605

692   Hofreiter, M., Jaenicke, V., Serre, D., Haeseler, A., & Pääbo, S. (2001). DNA sequences from multiple

693   amplifications reveal artifacts induced by cytosine deamination in ancient DNA. *Nucleic Acids Research*,

694   *29*. https://doi.org/10.1093/nar/29.23.4793

695   Hsieh, T. C., Ma, K. H., & Chao, A. (2016). iNEXT: an R package for rarefaction and extrapolation of species

696   diversity (Hill numbers). *Methods in Ecology and Evolution*, *7*(12), 1451–1456.

697   https://doi.org/10.1111/2041-210X.12613

698   Huang, S., Herzschuh, U., Pestryakova, L. A., Zimmermann, H. H., Davydova, P., Biskaborn, B. K., et al. (2020).

699   Genetic and morphologic determination of diatom community composition in surface sediments from

700   glacial and thermokarst lakes in the Siberian Arctic. *Journal of Paleolimnology*.

701   https://doi.org/10.1007/s10933-020-00133-1

702   Jakobsson, M., Pearce, C., Cronin, T. M., Backman, J., Anderson, L. G., Barrientos, N., et al. (2017). Post-glacial

703   flooding of the Bering Land Bridge dated to 11 cal ka BP based on new geophysical and sediment records.

704   *Climate of the Past*, *13*(8), 991–1005. https://doi.org/10.5194/cp-13-991-2017

705   Juggins, S. (2012). *rioja: Analysis of Quaternary science data, R package version 0.7-3*.

706   Kanz, C., Aldebert, P., Althorpe, N., Baker, W., Baldwin, A., Bates, K., et al. (2005). The EMBL nucleotide

707   sequence database. *Nucleic Acids Research*, *33*(DATABASE ISS.), 29–33.

708   https://doi.org/10.1093/nar/gki098

709   Katsuki, K., & Takahashi, K. (2005). Diatoms as paleoenvironmental proxies for seasonal productivity, sea-ice and

710   surface circulation in the Bering Sea during the late Quaternary. *Deep Sea Research Part II: Topical

711   Studies in Oceanography*, *52*(16), 2110–2130. https://doi.org/10.1016/j.dsr2.2005.07.001

712   Kruse, S. (2019). *R code for resampling and thus normalizing of count data to the minimum number of counts

713   across a set of samples (e.g. sedaDNA sequence/pollen taxa counts per sample along a sediment core)*.

714   Retrieved from https://github.com/StefanKruse/R_Rarefaction

715   Laskar, J., Robutel, P., Joutel, F., Gastineau, M., Correia, A. C. M., & Levrard, B. (2004). A long-term numerical

716   solution for the insolation quantities of the Earth. *Astronomy and Astrophysics*, *428*, 261–285.

717   https://doi.org/10.1051/0004-6361:20041335

718   Lepskaya, E. V., Jewson, D. H., & Usoltseva, M. V. (2010). *Aulacoseira subarctica* in Kurilskoye Lake,

719   Kamchatka: a deep, oligotrophic lake and important Pacific salmon nursery. *Diatom Research*, *25*(2), 323–

720   335. https://doi.org/10.1080/0269249X.2010.9705853

721   Levitan, M. A., Kuz'mina, T. G., Luksha, V. L., Roshchina, I. A., Syromyatnikov, K. V., Max, L., et al. (2015).

722   Evolution of sedimentation on the continental slope of the Kronotskii Peninsula (Eastern Kamchatka) over

723   the last 20 ka. *Lithology and Mineral Resources*, *50*(4), 249–269.

724   https://doi.org/10.1134/S0024490215040045

725   Li, W. K. W., McLaughlin, F. A., Lovejoy, C., & Carmack, E. C. (2009). Smallest algae thrive as the Arctic Ocean

726   freshens. *Science*, *326*(5952), 539–539. https://doi.org/10.1126/science.1179798

727   Limoges, A., Massé, G., Weckström, K., Poulin, M., Ellegaard, M., Heikkilä, M., et al. (2018). Spring succession

728   and vertical export of diatoms and IP$_{25}$ in a seasonally ice-covered high Arctic fjord. *Frontiers in Earth*

729   *Science*, *6*. https://doi.org/10.3389/feart.2018.00226

730   Lopes, C., Mix, A. C., & Abrantes, F. (2006). Diatoms in northeast Pacific surface sediments as paleoceanographic

731   proxies. *Marine Micropaleontology*, *60*(1), 45–65. https://doi.org/10.1016/j.marmicro.2006.02.010

732   Lovejoy, C., Legendre, L., Martineau, M.-J., Bâcle, J., & von Quillfeldt, C. H. (2002). Distribution of phytoplankton

733   and other protists in the North Water. *Deep Sea Research Part II: Topical Studies in Oceanography*,

734   *49*(22), 5027–5047. https://doi.org/10.1016/S0967-0645(02)00176-5

735   Matul', A. G., Saidova, Kh. M., Smirnova, M. A., Khusid, T. A., Kazarina, G. Kh., & Chekhovskaya, M. P. (2015).

736   Rapid diachronous paleoceanographic changes in the Far East marginal areas of the Pacific Ocean at the

737   last glaciation-to-holocene transition. *Doklady Earth Sciences*, *463*(2), 873–877.

738   https://doi.org/10.1134/S1028334X1508022X

739   Max, L., Riethdorf, J.-R., Tiedemann, R., Smirnova, M., Lembke-Jene, L., Fahl, K., et al. (2012a). Biogenic opal of

740   sediment core SO201-2-12 [Data set]. *In supplement to: Max, L et al. (2012): Sea surface temperature*

741   *variability and sea-ice extent in the subarctic northwest Pacific during the past 15,000 years.*

742   *Paleoceanography, 27(3), PA3213, https://doi.org/10.1029/2012PA002292*. PANGAEA.

743   https://doi.org/10.1594/PANGAEA.786197

744   Max, L., Riethdorf, J.-R., Tiedemann, R., Smirnova, M., Lembke-Jene, L., Fahl, K., et al. (2012b). Sea surface

745   temperature calculated from alkenones of sediment core SO201-2-12 [Data set]. *In supplement to: Max, L*

746   *et al. (2012): Sea surface temperature variability and sea-ice extent in the subarctic northwest Pacific*

747   *during the past 15,000 years. Paleoceanography, 27(3), PA3213, https://doi.org/10.1029/2012PA002292*.

748   PANGAEA. https://doi.org/10.1594/PANGAEA.786132

749   Max, L., Riethdorf, J.-R., Tiedemann, R., Smirnova, M., Lembke-Jene, L., Fahl, K., et al. (2012). Sea surface

750   temperature variability and sea-ice extent in the subarctic northwest Pacific during the past 15,000 years.

751   *Paleoceanography*, *27*(3). https://doi.org/10.1029/2012PA002292

752   McQuoid, M. R., & Nordberg, K. (2003). The diatom Paralia sulcata as an environmental indicator species in

753   coastal sediments. *Estuarine, Coastal and Shelf Science*, *56*(2), 339–354. https://doi.org/10.1016/S0272-

754   7714(02)00187-7

755   Medlin, L. K., & Hasle, G. R. (1990). Some *Nitzschia* and related diatom species from fast ice samples in the Arctic

756   and Antarctic. *Polar Biology*, *10*(6). https://doi.org/10.1007/BF00233693

757   Méheust, M., Stein, R., Fahl, K., Max, L., & Riethdorf, J.-R. (2015). High-resolution IP25 of sediment core SO201-

758   2-12 [Data set]. *In supplement to: Méheust, M et al. (2015): High-resolution IP25-based reconstruction of*

759   *sea-ice variability in the western North Pacific and Bering Sea during the past 18,000 years. Geo-Marine*

760   *Letters, https://doi.org/10.1007/s00367-015-0432-4*. PANGAEA.

761   https://doi.org/10.1594/PANGAEA.855451

762   Méheust, M., Stein, R., Fahl, K., Max, L., & Riethdorf, J.-R. (2016). High-resolution IP25-based reconstruction of

763   sea-ice variability in the western North Pacific and Bering Sea during the past 18,000 years. *Geo-Marine*

764   *Letters*, *36*(2), 101–111. https://doi.org/10.1007/s00367-015-0432-4

765   Meiners, K., Krembs, C., & Gradinger, R. (2008). Exopolymer particles: microbial hotspots of enhanced bacterial

766   activity in Arctic fast ice (Chukchi Sea). *Aquatic Microbial Ecology*, *52*(2), 195–207.

767   https://doi.org/10.3354/ame01214

768   Meyer, V. D., Max, L., Hefter, J., Tiedemann, R., & Mollenhauer, G. (2016a). Fractional abundances of isoprenoid

769   and branched glycerol dialkyl glycerol tetraethers (GDGT) of sediment core SO201-2-12KL [Data set]. *In*

770   *supplement to: Meyer, VD et al. (2016): Glacial-to-Holocene evolution of sea surface temperature and*

771   *surface circulation in the subarctic northwest Pacific and the Western Bering Sea. Paleoceanography, 31,*

772   *12 pp, https://doi.org/10.1002/2015PA002877*. PANGAEA. https://doi.org/10.1594/PANGAEA.862964

773   Meyer, V. D., Max, L., Hefter, J., Tiedemann, R., & Mollenhauer, G. (2016b). Glacial-to-Holocene evolution of sea

774   surface temperature and surface circulation in the subarctic northwest Pacific and the Western Bering Sea.

775   *Paleoceanography*, *31*(7), 916–927. https://doi.org/10.1002/2015PA002877

776   Meyer, V. D., Hefter, J., Lohmann, G., Max, L., Tiedemann, R., & Mollenhauer, G. (2017). Summer temperature

777   evolution on the Kamchatka Peninsula, Russian Far East, during the past 20 000 years. *Climate of the Past*,

778   *13*(4), 359–377. https://doi.org/10.5194/cp-13-359-2017

779   Nagano, A., Wakita, M., & Watanabe, S. (2016). Dichothermal layer deepening in relation with halocline depth

780   change associated with northward shrinkage of North Pacific western subarctic gyre in early 2000s. *Ocean*

781   *Dynamics*, *66*(2), 163–172. https://doi.org/10.1007/s10236-015-0917-8

782   Nummelin, A., Ilicak, M., Li, C., & Smedsrud, L. H. (2016). Consequences of future increased Arctic runoff on

783   Arctic Ocean stratification, circulation, and sea ice cover. *Journal of Geophysical Research: Oceans*,

784   *121*(1), 617–637. https://doi.org/10.1002/2015JC011156

785   Oksanen, J., Blanchet, F. G., Kindt, R., Legendre, P., Minchin, P. R., O´Hara, R. B., et al. (2011). *vegan:*

786   *Community Ecology Package. R package version 2.0-2.*

787   Olsen, L. M., Duarte, P., Peralta-Ferriz, C., Kauko, H. M., Johansson, M., Peeken, I., et al. (2019). A red tide in the

788   pack ice of the Arctic Ocean. *Scientific Reports*, *9*. https://doi.org/10.1038/s41598-019-45935-0

789   Pääbo, S. (1989). Ancient DNA: extraction, characterization, molecular cloning, and enzymatic amplification.

790   *Proceedings of the National Academy of Sciences of the United States of America*, *86*(6), 1939–1943.

791   Parkinson, C. L., Cavalieri, D. J., Gloersen, P., Zwally, H. J., & Comiso, J. C. (1999). Arctic sea ice extents, areas,

792   and trends, 1978–1996. *Journal of Geophysical Research: Oceans*, *104*(C9), 20837–20856.

793   https://doi.org/10.1029/1999JC900082

794   Pawłowska, J., Łącka, M., Kucharska, M., Pawlowski, J., & Zajączkowski, M. (2020). Multiproxy evidence of the

795   Neoglacial expansion of Atlantic Water to eastern Svalbard. *Climate of the Past*, *16*(2), 487–501.

796   https://doi.org/10.5194/cp-16-487-2020

797   Pistone, K., Eisenman, I., & Ramanathan, V. (2014). Observational determination of albedo decrease caused by

798   vanishing Arctic sea ice. *Proceedings of the National Academy of Sciences*, *111*(9), 3322–3326.

799   https://doi.org/10.1073/pnas.1318201111

800   Polyakova, A. M. (2007). Extreme supply of floating ice to the northwestern part of the Pacific Ocean. *Oceanology*,

801   *47*(1), 1–4. https://doi.org/10.1134/S0001437007010018

802   Poulin, M., Daugbjerg, N., Gradinger, R., Ilyash, L., Ratkova, T., & Quillfeldt, C. von. (2011). The pan-Arctic

803   biodiversity of marine pelagic and sea-ice unicellular eukaryotes: a first-attempt assessment. *Marine*

804   *Biodiversity*, *41*(1), 13–28. https://doi.org/10.1007/s12526-010-0058-8

805   von Quillfeldt, C. H. (1997). Distribution of diatoms in the Northeast Water Polynya, Greenland. *Journal of Marine*

806   *Systems*, *10*(1), 211–240. https://doi.org/10.1016/S0924-7963(96)00056-5

807   von Quillfeldt, C. H. (2000). Common diatom species in Arctic spring blooms: their distribution and abundance.

808   *Botanica Marina*, *43*(6). https://doi.org/10.1515/BOT.2000.050

809   R Core Team. (2018). *R: A language and environment for statistical computing*. Vienna, Austria: R Foundation for

810   Statistical Computing. Retrieved from https://www.R-project.org/

811   Rasmussen, S. O., Bigler, M., Blockley, S. P., Blunier, T., Buchardt, S. L., Clausen, H. B., et al. (2014). A

812   stratigraphic framework for abrupt climatic changes during the Last Glacial period based on three

813   synchronized Greenland ice-core records: refining and extending the INTIMATE event stratigraphy.

814   *Quaternary Science Reviews*, *106*, 14–28. https://doi.org/10.1016/j.quascirev.2014.09.007

815   Ren, J., Jiang, H., Seidenkrantz, M.-S., & Kuijpers, A. (2009). A diatom-based reconstruction of Early Holocene

816   hydrographic and climatic change in a southwest Greenland fjord. *Marine Micropaleontology*, *70*(3–4),

817   166–176. https://doi.org/10.1016/j.marmicro.2008.12.003

818   Ren, J., Gersonde, R., Esper, O., & Sancetta, C. (2014). Diatom distributions in northern North Pacific surface

819   sediments and their relationship to modern environmental variables. *Palaeogeography, Palaeoclimatology,*

820   *Palaeoecology*, *402*, 81–103. https://doi.org/10.1016/j.palaeo.2014.03.008

821   Reschke, M., Kunz, T., & Laepple, T. (2019). Comparing methods for analysing time scale dependent correlations

822   in irregularly sampled time series data. *Computers & Geosciences*, *123*, 65–72.

823   https://doi.org/10.1016/j.cageo.2018.11.009

824   Riethdorf, J.-R., Max, L., Nürnberg, D., Lembke-Jene, L., & Tiedemann, R. (2013a). Deglacial development of

825   (sub) sea surface temperature and salinity in the subarctic northwest Pacific: Implications for upper-ocean

826   stratification: deglacial subsurface temperature and salinity in the NW Pacific. *Paleoceanography*, *28*(1),

827   91–104. https://doi.org/10.1002/palo.20014

828   Riethdorf, J.-R., Max, L., Nürnberg, D., Lembke-Jene, L., & Tiedemann, R. (2013b). Stable isotopes measured on

829   benthic foraminifers of sediment core SO201-2-12 [Data set]. *In supplement to: Riethdorf, J-R et al.*

830   *(2013): Deglacial development of (sub) sea surface temperature and salinity in the subarctic northwest*

831   *Pacific: Implications for upper-ocean stratification. Paleoceanography, 28(1), 91-104,*

832   *https://doi.org/10.1002/palo.20014*. PANGAEA. https://doi.org/10.1594/PANGAEA.786246

833 Rimet, F., Gusev, E., Kahlert, M., Kelly, M. G., Kulikovskiy, M., Maltsev, Y., et al. (2019). Diat.barcode, an open-

834   access curated barcode library for diatoms. *Scientific Reports*, *9*(1), 15116. https://doi.org/10.1038/s41598-

835   019-51500-6

836 Rotatore, C., Colman, B., & Kuzma, M. (1995). The active uptake of carbon dioxide by the marine diatoms

837   *Phaeodactylum ticornutum* and *Cyclotella* sp. *Plant, Cell & Environment*, *18*(8), 913–918.

838   https://doi.org/10.1111/j.1365-3040.1995.tb00600.x

839 Round, F. E., Crawford, R. M., & Mann, D. G. (1990). *Diatoms: Biology and morphology of the genera*. Cambridge

840   University Press.

841 Sancetta, C. (1979). Oceanography of the North Pacific during the last 18,000 years: Evidence from fossil diatoms.

842   *Marine Micropaleontology*, *4*, 103–123. https://doi.org/10.1016/0377-8398(79)90009-4

843 Sancetta, C. (1982). Distribution of diatom species in surface sediments of the Bering and Okhotsk Seas.

844   *Micropaleontology*, *28*(3), 221–257. https://doi.org/10.2307/1485181

845 Sancetta, C., & Silvestri, S. (1986). Pliocene-Pleistocene evolution of the North Pacific Ocean-Atmosphere system,

846   interpreted from fossil diatoms. *Paleoceanography*, *1*(2), 163–180.

847   https://doi.org/10.1029/PA001i002p00163

848 Schlitzer, R. (2002). Interactive analysis and visualization of geoscience data with Ocean Data View,

849   https://odv.awi.de. *Computers & Geosciences*, *28*(10), 1211–1218. https://doi.org/10.1016/S0098-

850   3004(02)00040-7

851 Schnell, I. B., Bohmann, K., & Gilbert, M. T. P. (2015). Tag jumps illuminated – reducing sequence-to-sample

852   misidentifications in metabarcoding studies. *Molecular Ecology Resources*, *15*(6), 1289–1303.

853   https://doi.org/10.1111/1755-0998.12402

854 Shu, Q., Qiao, F., Song, Z., Zhao, J., & Li, X. (2018). Projected freshening of the Arctic Ocean in the 21st century.

855   *Journal of Geophysical Research: Oceans*, *123*(12), 9232–9244. https://doi.org/10.1029/2018JC014036

856 Smirnova, M. A., Kazarina, G. Kh., Matul, A. G., & Max, L. (2015). Diatom evidence for paleoclimate changes in

857   the northwestern Pacific during the last 20000 years. *Oceanology*, *55*(3), 383–389.

858   https://doi.org/10.1134/S0001437015030157

859 Stabell, B. (1986). A diatom maximum horizon in upper Quaternary deposits. *Geologische Rundschau*, *75*(1), 175–

860   184. https://doi.org/10.1007/BF01770186

861   Stabeno, P. J., & Reed, R. K. (1994). Circulation in the Bering Sea Basin Observed by Satellite-Tracked Drifters:

862   1986–1993. *Journal of Physical Oceanography*, *24*(4), 848–854. https://doi.org/10.1175/1520-

863   0485(1994)024<0848:CITBSB>2.0.CO;2

864   Stabeno, P. J., Schumacher, J. D., & Ohtani, K. (1999). The physical oceanography of the Bering Sea. In T. R.

865   Loughlin & K. Ohtani (Eds.), *Dynamics of the Bering Sea: A summary of physical, chemical, and*

866   *biological characteristics, and a synopsis of research on the Bering Sea* (pp. 1–28). University of Alaska

867   Sea Grant, Fairbanks: North Pacific Marine Science Organization. Retrieved from

868   https://www.pmel.noaa.gov/pubs/outstand/stab1878/stab1878.shtml

869   Stoof-Leichsenring, K. R., Epp, L. S., Trauth, M. H., & Tiedemann, R. (2012). Hidden diversity in diatoms of

870   Kenyan Lake Naivasha: a genetic approach detects temporal variation. *Molecular Ecology*, *21*(8), 1918–

871   1930. https://doi.org/10.1111/j.1365-294X.2011.05412.x

872   Syvertsen, E. E. (1991). Ice algae in the Barents Sea: types of assemblages, origin, fate and role in the ice-edge

873   phytoplankton bloom. *Polar Research*, *10*(1), 277–288. https://doi.org/10.1111/j.1751-

874   8369.1991.tb00653.x

875   Tremblay, J.-É., & Gagnon, J. (2009). The effects of irradiance and nutrient supply on the productivity of Arctic

876   waters: a perspective on climate change. In J. C. J. Nihoul & A. G. Kostianoy (Eds.), *Influence of Climate*

877   *Change on the Changing Arctic and Sub-Arctic Conditions* (pp. 73–93). Dordrecht: Springer Netherlands.

878   https://doi.org/10.1007/978-1-4020-9460-6_7

879   Vincent, F., & Bowler, C. (2020). Diatoms are selective segregators in global ccean planktonic communities.

880   *MSystems*, *5*(1). https://doi.org/10.1128/mSystems.00444-19

881   Walsh, J. E., Fetterer, F., stewart, J. S., & Chapman, W. L. (2017). A database for depicting Arctic sea ice variations

882   back to 1850. *Geographical Review*, *107*(1), 89–107. https://doi.org/10.1111/j.1931-0846.2016.12195.x

883   Zimmermann, H. H., Raschke, E., Epp, L. S., Stoof-Leichsenring, K. R., Schwamborn, G., Schirrmeister, L., et al.

884   (2017). Sedimentary ancient DNA and pollen reveal the composition of plant organic matter in Late

885   Quaternary permafrost sediments of the Buor Khaya Peninsula (north-eastern Siberia). *Biogeosciences*,

886   *14*(3), 575–596. https://doi.org/10.5194/bg-14-575-2017

887   Zimmermann, H. H., Stoof-Leichsenring, K. R., Kruse, S., Müller, J., Stein, R., Tiedemann, R., & Herzschuh, U.

888   (2019). Changes in the composition of marine and sea-ice diatoms derived from sedimentary ancient DNA

889   of the eastern Fram Strait over the past 30,000 years. *Ocean Science Discussions*, 1–25.

890   https://doi.org/10.5194/os-2019-113

891   Zimmermann, H. H., Stoof-Leichsenring, K. R., Kruse, S., Nuernberg, D., Tiedemann, R., & Herzschuh, U. (2020).

892   Diatom sedimentary ancient DNA metabarcoding from Kronotsky Peninsula. *Dryad, Dryad Dataset*.

893   https://doi.org/10.5061/dryad.qnk98sfdh

894   Zimmermann, H. H., Stoof-Leichsenring, K. R., Kruse, S., Müller, J., Stein, R., Tiedemann, R., & Herzschuh, U.

895   (2020). Diatom sedimentary ancient DNA metabarcoding from western Fram Strait and Kronotsky

896   Peninsula. *Dryad, Dryad Dataset*. https://doi.org/10.5061/dryad.bnzs7h481

897   Zimmermann, J., Abarca, N., Enk, N., Skibbe, O., Kusber, W.-H., & Jahn, R. (2014). Taxonomic reference libraries

898   for environmental barcoding: A best practice example from diatom research. *PLoS ONE*, *9*(9), e108793.

899   https://doi.org/10.1371/journal.pone.0108793

900